X-Ray and Neutron Diffraction of Amorphous Nickel-Zirconium-Alloys as Prepared in Different Ways

W.-M. Kuschke, L. Schultz*, P. Lamparter, and S. Steeb

Max-Planck-Institut für Metallforschung, Institut für Werkstoffwissenschaft, Stuttgart

Z. Naturforsch. **46a**, 491–498 (1991); received February 25, 1991

The structure of amorphous Ni_xZr_{100-x}-alloys ($x = 30$, 31, 34, 63.7, and 65), which were produced by melt spinning (MS), mechanical alloying (MA), and sputtering (SP) was studied by X-ray- and neutron diffraction yielding structure factors, pair correlation functions, coordination numbers, atomic distances, and Warren-Cowley chemical short range order parameters. The atomic arrangement within the first coordination sphere is independent of the method of preparation while in the second and higher spheres it differs between the MS- and the MA-alloys on the one side and the SP-specimens on the other side. Thus one understands that some physical properties of the different specimens differ.

1. Introduction

In the present paper we investigate the short range order structure of amorphous $Ni_xZr_{(100-x)}$-alloys ($x = 30$, 31, 34, 63.7, and 65) and focus on the question whether there exists an influence on the atomic arrangement of the production method, namely melt-spinning, mechanical alloying, and sputtering.

2. Theoretical

We refer to reference [1] concerning the theoretical fundamentals of structural investigations and the definition of the Faber-Ziman structure factor $S^{FZ}(Q)$, where $Q = 4\pi(\sin\Theta)/\lambda$, λ = wavelength, 2Θ = scattering angle, as well as the definition of the Bhatia-Thornton structure factor $S^{BT}(Q)$, the Faber-Ziman pair correlation function $G(R)$, the pair distribution function $g(R)$, and the Warren-Cowley short range order parameter

$$\alpha = \frac{Z_{AA} - Z \cdot c_A}{Z \cdot c_B}, \tag{1}$$

where

Z_{AA} = number of A-atoms around an A-atom, in a binary alloy A–B,

Z = mean coordination number in the alloy,

c_i = concentration of atoms of kind i in atomic fractions.

3. Experimental

3.1. Preparation of Specimens

In the following, MS, MA, and SP stand for melt-spinning, mechanical alloying, and sputtering, respectively.

3.1.1. MS-Specimens

We used two amorphous alloys produced by MS, namely MS-$Ni_{31}Zr_{69}$ and MS-$Ni_{34}Zr_{66}$. MS was done in He-atmosphere (100 mbar). The Cu-cylinder with a diameter of 30 cm rotated with 50 s^{-1}. The melt was contained in quartz cylinders with 0.7 mm ejection hole diameter at a distance of 3 mm from the cylinder. The amorphous ribbons were 20 to 30 µm thick and 0.8 to 1 mm wide.

3.1.2. MA-Specimens

The MA-specimens MA-$Ni_{30}Zr_{70}$ and MA-$Ni_{65}Zr_{35}$ were produced within an inert Ar-atmosphere containing less than 1 ppm O_2 and H_2O starting from Ni- and Zr-powders with typical particle diameters of about 40 µm. Milling was done during 60 h in intervals of 15 min milling and 15 min pause [2].

* Siemens AG, Research Laboratories, W-8520 Erlangen.

Reprint requests to Prof. Dr. S. Steeb, Institut für Werkstoffwissenschaft, Max-Planck-Institut für Metallforschung, Seestraße 91, W-7000 Stuttgart 10.

0932-0784 / 91 / 0600-0491 $ 01.30/0. – Please order a reprint rather than making your own copy.

3.1.3. SP-Specimen

The SP-$Ni_{34}Zr_{66}$-specimen (thickness 50 μm) was produced within a sputter-unit (Z 400, Leybold-Heraeus) on 6.2 μm thick mylar foil. During sputtering the substrate was water-cooled. The experimental parameters to obtain an amorphous specimen are 10^{-2} mbar Ar, high voltage 1.3 kV, cathode current 125 mA, DC-potential 1.2 kV, frequency 13.56 MHz, and sputtering time 72 h. The mylar foil does not disturb the X-ray diffraction work.

3.2. Diffraction Apparatus

3.2.1. X-Ray Diffraction

X-ray diffraction was done using molybdenum radiation with the instrument D 500 (Fa. Siemens) in transmission mode. A quartz monochromator was used in the primary beam. The radiation is detected using a scintillation counter. The amorphous ribbons and the mylar foil with the SP-specimen were fixed onto frames.

3.2.2. Neutron Diffraction

Neutron diffraction was done at the Institute Laue-Langevin, Grenoble, using the two-axes-diffractometers D4 and D20.

With D4 we used the wavelength 0.7 Å which allowed a Q-region between 0.2 $Å^{-1}$ and 16 $Å^{-1}$. With D20 we used the wavelength $\lambda = 0.87$ Å and thus had available the Q-region from 0.5 $Å^{-1}$ up to 14 $Å^{-1}$.

The specimens were filled into cylinders made from vanadium foils (outer diameter 7 mm, wall thickness 75 μm). According to [3] for the two elements Ni and Zr the scattering lengths b, the scattering cross sections σ_s, and the absorption cross sections σ_a for the wavelength $\lambda = 0.7$ Å amount to the values given in Table 1.

Table 1. Scattering length b, scattering cross section σ_s, and absorption cross section σ_a for $\lambda = 0.7$ Å according to [3].

Element	b [10^{-12} cm]	σ_s [10^{-24} cm^2]	σ_a [10^{-24} cm^2]
Ni	1.03	17.56	1.75
Zr	0.716	6.56	0.07

4. Results and Discussion

4.1. MS-$Ni_{31}Zr_{69}$ and MA-$Ni_{30}Zr_{70}$; Neutron Diffraction

Both specimens were investigated using the diffractometer D4 at ILL, Grenoble, using the wavelength 0.7 Å.

4.1.1. MS-$Ni_{31}Zr_{69}$

Figure 1 shows the experimental intensity versus the scattering angle 2Θ. With increasing 2Θ values the mean intensity decreases, i.e. it does not oscillate around a horizontal line as it should with neutron diffraction. This decrease is stronger than explicable by the inelastic scattering effect from the Ni-Zr alloy and is caused by hydrogen. Thus the intensity curve had to be corrected using a normalized intensity curve for hydrogen as described in [4]. During the correction method it became evident that the specimen contained 2 atom percent hydrogen.

Figure 2 shows the Faber Ziman structure factor S^{FZ} with a distinct premaximum at $Q = 1.7$ $Å^{-1}$, which is a strong hint on compound formation. Fourier transformation of the structure factor yields the pair correlation function $G(R)$ with its split up main maximum at $R = 2.68$ Å and 3.18 Å as shown in Fig. 3 by the dotted curve.

According to [5] the Goldschmidt diameters for Ni and Zr amount to 2.49 Å and 3.19 Å, respectively. Thus the maximum at 3.18 Å can be attributed to the Zr–Zr-correlation. To explain the maximum at 2.68 Å we need the equation

$$G^{tot}_{Ni_{31}Zr_{69}} = 0.14\, G_{NiNi} + 0.47\, G_{NiZr} + 0.38\, G_{ZrZr} \qquad (2)$$

which shows how to split up the total pair correlation function G^{tot} into the three partial functions G_{NiNi}, G_{NiZr}, and G_{ZrZr}.

Furthermore we use the shortest Ni–Zr-distances in crystalline $Ni_{50}Zr_{50}$ from [6] which amount to 2.66 Å, 2.70 Å, and 2.87 Å. If we assume the Ni–Zr-distance in amorphous MS-$Ni_{31}Zr_{69}$ to be as small as the shortest Ni–Zr-distance in crystalline $Ni_{50}Zr_{50}$, then we can attribute the experimental R-value of 2.68 Å to the Ni–Zr-correlation. An interpretation as Ni–Ni distance, which would be expected at 2.49 Å, can be excluded because of the small weighting factor of only 0.14.

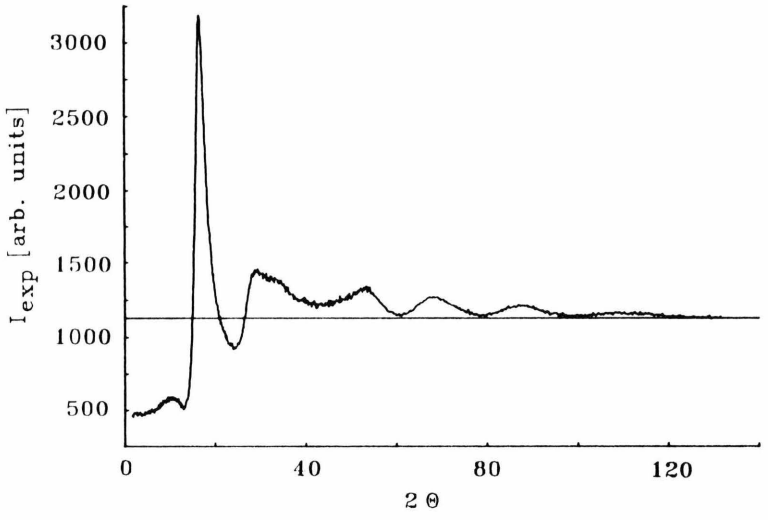

Fig. 1. MS-$Ni_{31}Zr_{69}$; neutron diffraction ($\lambda = 0.7$ Å); exp. intensity after corrections for absorption, container- and background-contribution.

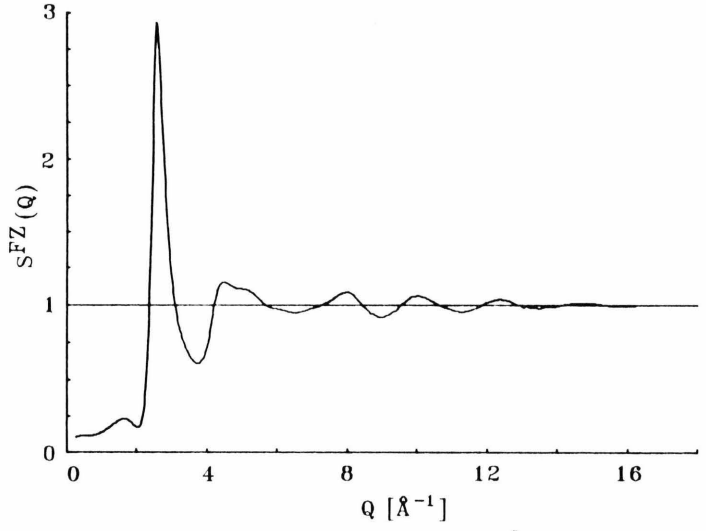

Fig. 2. MS-$Ni_{31}Zr_{69}$; neutron diffraction ($\lambda = 0.7$ Å); structure factor according to Faber Ziman.

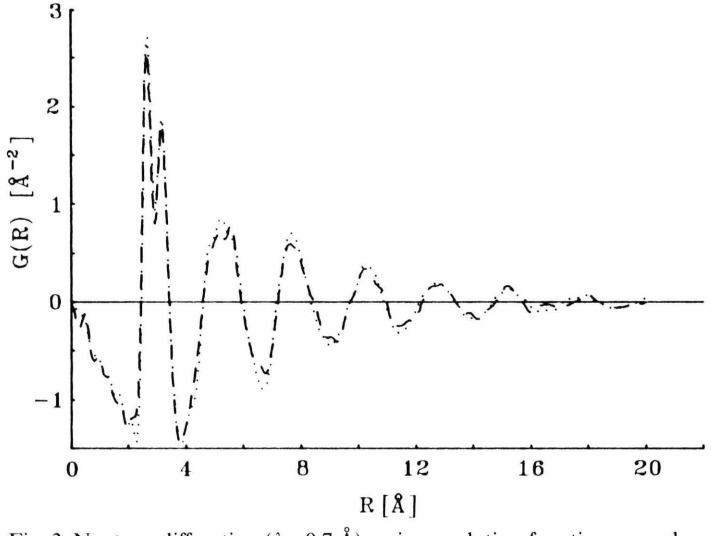

Fig. 3. Neutron diffraction ($\lambda = 0.7$ Å); pair correlation function according to Faber Ziman. MS-$Ni_{31}Zr_{69}$ (· · · · ·); MA-$Ni_{30}Zr_{70}$ (– – –).

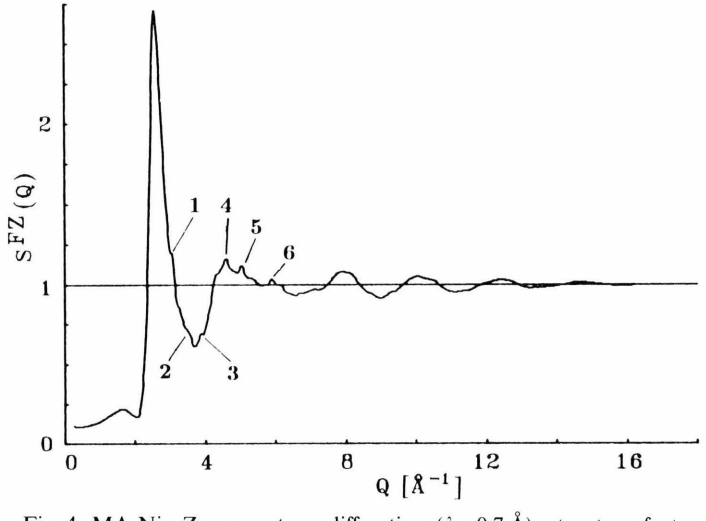

Fig. 4. MA-$Ni_{30}Zr_{70}$; neutron diffraction ($\lambda = 0.7$ Å); structure factor according to Faber Ziman. For numbering see text.

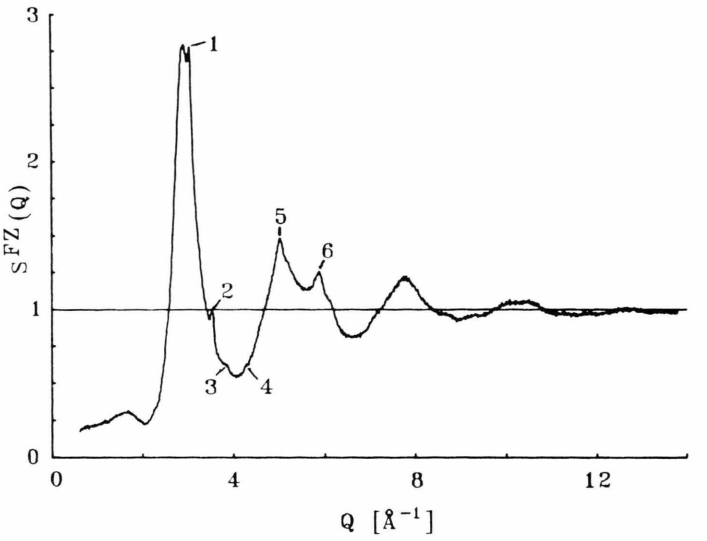

Fig. 5. MA-$Ni_{65}Zr_{35}$; neutron diffraction ($\lambda = 0.87$ Å); structure factor according to Faber Ziman. For numbering see text.

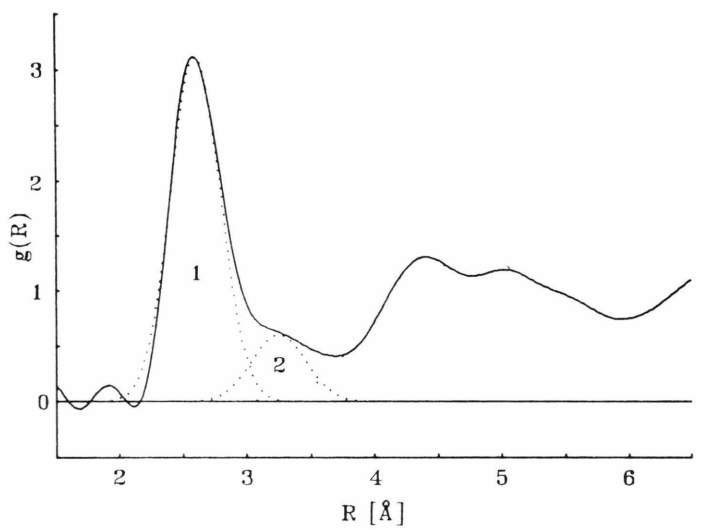

Fig. 6. MA-$Ni_{65}Zr_{35}$; neutron diffraction ($\lambda = 0.87$ Å); pair distribution function with Gauss fit.

4.1.2. MA-$Ni_{30}Zr_{70}$

Also in this case a correction for hydrogen scattering had to be applied corresponding to a hydrogen content of about 1.7 atom percent. Figure 4 shows the Faber-Ziman structure factor. The small peaks marked with numbers show that the specimen contains crystalline residuals which are Ni (peaks 1, 2, 5, and 6) and α-Zr (peaks 3 and 4). The corresponding pair correlation function is shown in Fig. 3 with a dashed line and compared with that obtained with MS-$Ni_{31}Zr_{69}$ (dotted line). $G(R)$ obtained with MA-$Ni_{30}Zr_{70}$ also shows pronounced peaks at 2.68 Å and 3.18 Å and a run very similar to that of $G(R)$ obtained with MS-$Ni_{31}Zr_{69}$.

From the corresponding $g(R)$-curves we obtained by fitting with Gauss curves for the first and second maximum at 2.68 Å and 3.18 Å the coordination numbers as given in Table 2.

As a result we state a strong similarity of the short range structure in the two amorphous specimens MS-$Ni_{31}Zr_{69}$ and MA-$Ni_{30}Zr_{70}$.

Table 2. MS-$Ni_{31}Zr_{69}$ and MA-$Ni_{30}Zr_{70}$; coordination numbers.

Specimen	Z_{NiZr}	Z_{ZrZr}
MS-$Ni_{31}Zr_{69}$	5.9	11.7
MA-$Ni_{30}Zr_{70}$	5.9	11.4

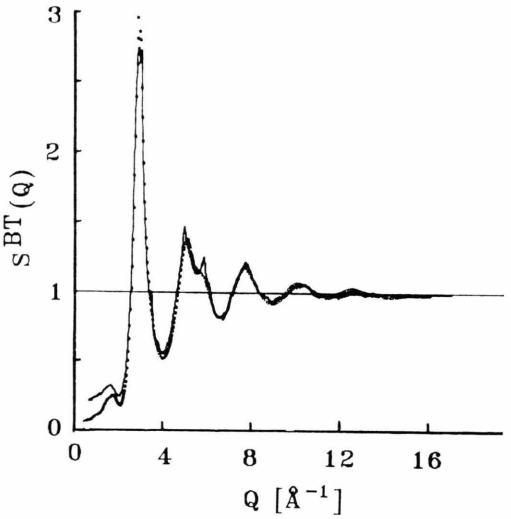

Fig. 7. MS-$Ni_{63.7}Zr_{36.3}$ (· · · ·) and MA-$Ni_{65}Zr_{35}$ (——); neutron diffraction ($\lambda = 0.87$ Å); structure factor $S^{BT}(Q)$ according to Bhatia and Thornton.

4.2. MA-$Ni_{65}Zr_{35}$ and MS-$Ni_{63.7}Zr_{36.3}$; Neutron Diffraction

4.2.1. MA-$Ni_{65}Zr_{35}$

This specimen was investigated using the diffractometer D 20 at ILL, Grenoble with 0.87 Å wavelength.

The intensity curve as obtained with the MA-$Ni_{65}Zr_{35}$-specimen oscillates rather well around a horizontal line and thus had not to be corrected for hydrogen contamination. Figure 5 shows the Faber Ziman structure factor which contains small Bragg-peaks which can be attributed to crystalline impurities, namely Ni (1, 2, 5, and 6) and α-Zr (3 and 4).

In Fig. 6 we present the total distribution function $g(R)$ as obtained from the structure factor in Fig. 5 in the region 1.5 Å $\leq R \leq$ 6.5 Å. The main maximum lies at 2.59 Å. The total distribution function is composed of the partial functions according to

$$g^{tot}_{Ni_{65}Zr_{35}} = 0.529\, g_{NiNi} + 0.396\, g_{NiZr} + 0.074\, g_{ZrZr}\,. \quad (3)$$

The three weighting factors show that the Ni–Ni- and Ni–Zr-partial distributions are weighted with nearly the same coefficient, whereas the weighting factor of g_{ZrZr} only amounts to 0.074. According to Goldschmidt we expect for the Ni–Ni-distance and the Ni–Zr-distance 2.49 Å and 2.84 Å, respectively. The nearest Ni–Zr distance in crystalline $Ni_{50}Zr_{50}$ amounts to 2.66 Å. All these distances lie in the range of the maximum 1 which therefore is attributed to Ni–Ni- and Ni–Zr-distances. The fitting of Gauss curves to the maximum in Fig. 6 yields a small maximum 2 at 3.25 Å which can be ascribed to Zr–Zr-pairs.

Table 3. MA-$Ni_{65}Zr_{35}$, coordination numbers.

Gauss-peak	Z_{ZrZr}	Z_{NiNi}	Z_{NiZr}
1	–	6	6.1
2	5.6	–	–

4.2.2. MS-$Ni_{63.7}Zr_{36.3}$

We use the data given in [7], which were obtained with MS-$Ni_{63.7}Zr_{36.3}$, for comparison with MA-$Ni_{65}Zr_{35}$. Figure 7 shows the Bhatia-Thornton structure factors as abtained from both specimens. Both $S^{BT}(Q)$-curves coincide very well, especially looking at the Q-region around 1.5 Å^{-1} where in both cases a premaximum is observed. This means that in the two specimens MA-$Ni_{65}Zr_{35}$ and MS-$Ni_{63.7}Zr_{36.3}$ exists a very similar chemical short range order. In [7] for MS-$Ni_{63.7}Zr_{36.3}$ in the region of the first coordination sphere the partial coordination numbers $Z_{NiNi} = 6$, $Z_{NiZr} = 5$, and $Z_{ZrZr} = 5.84$ were reported. These are nearly the same coordination numbers as obtained during the present work by splitting maximum 1 in Fig. 6 into two Gaussians (see Table 3).

4.3. MS-$Ni_{34}Zr_{66}$ and SP-$Ni_{34}Zr_{66}$; X-Ray Diffraction

Both specimens were investigated using the diffractometer D 500 with a resolution in 2Θ of 0.2°. The formfactors and coefficients of anomalous dispersion were taken from [8, 9].

4.3.1. MS-$Ni_{34}Zr_{66}$

Figure 8 shows the Faber Ziman structure factor and Fig. 9 the corresponding pair correlation function with a split up main maximum. The distances 2.68 Å and 3.20 Å correspond to those obtained with neutron diffraction with specimens of similar composition (Sect. 4.1) and are ascribed to Ni–Zr and Zr–Zr, respectively.

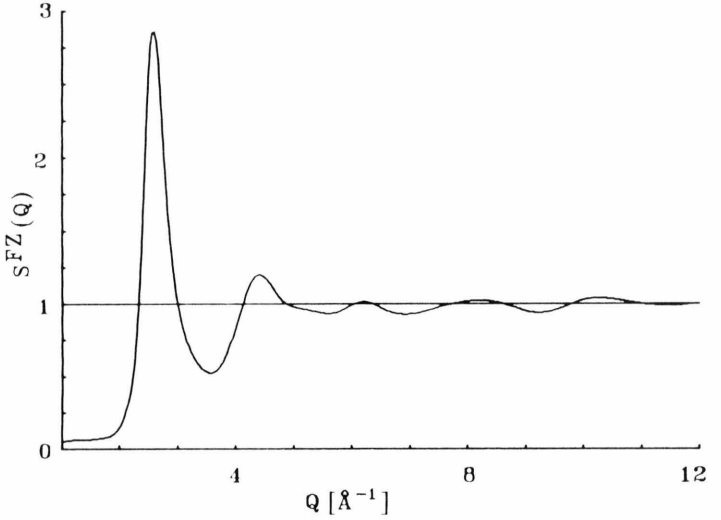

Fig. 8. MS-$Ni_{34}Zr_{66}$; X-ray diffraction (Mo-Kα); structure factor according to Faber-Ziman.

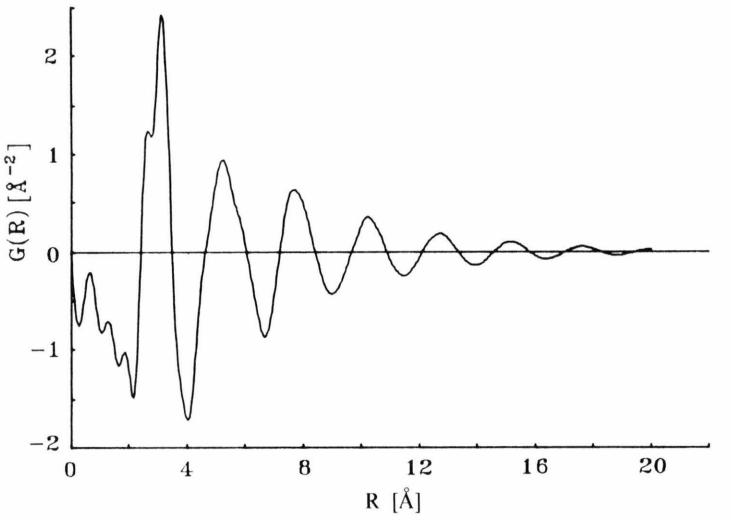

Fig. 9. MS-$Ni_{34}Zr_{66}$; X-ray diffraction (Mo-Kα); pair correlation function.

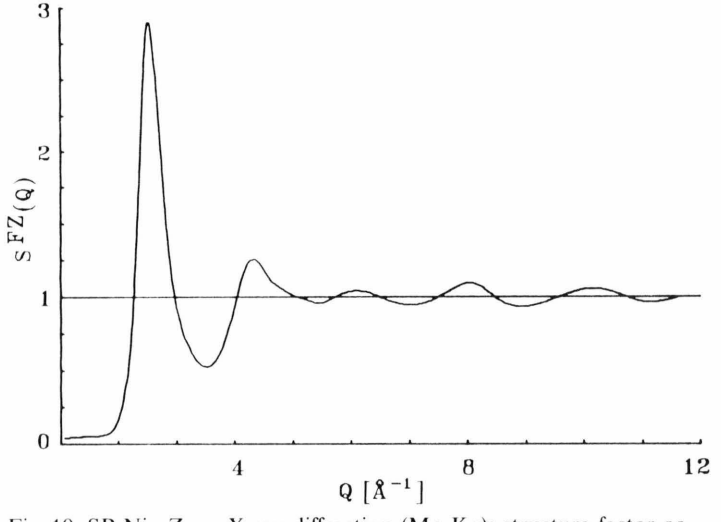

Fig. 10. SP-$Ni_{34}Zr_{66}$; X-ray diffraction (Mo-Kα); structure factor according to Faber-Ziman.

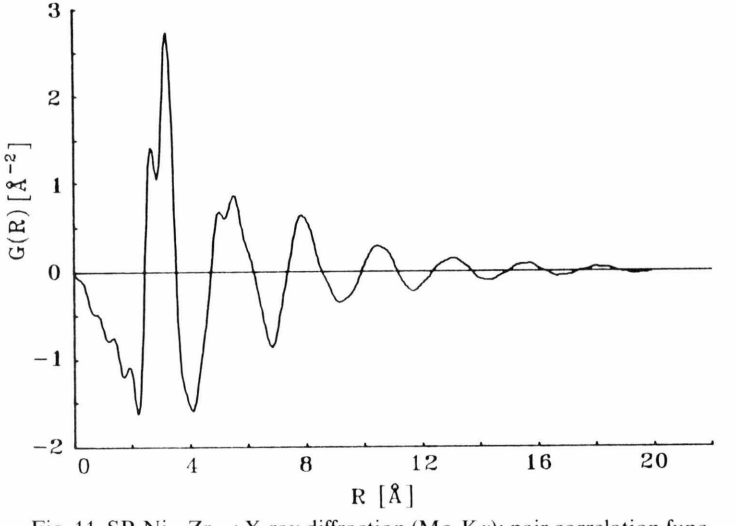

Fig. 11. SP-$Ni_{34}Zr_{66}$; X-ray diffraction (Mo-Kα); pair correlation function.

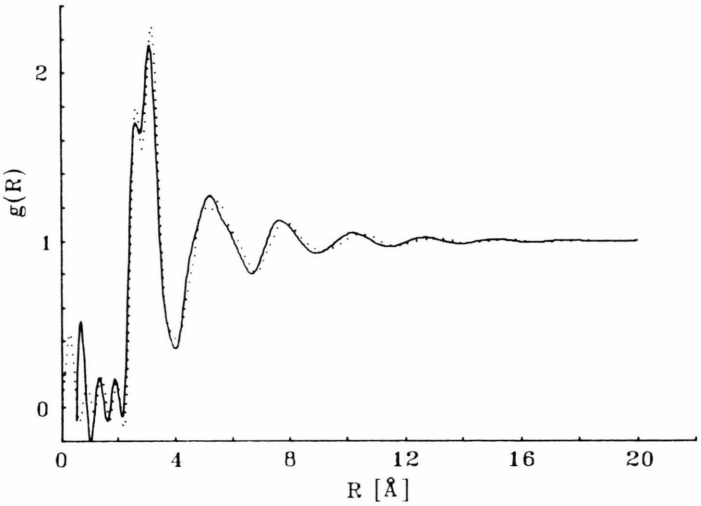

Fig. 12. MS-$Ni_{34}Zr_{66}$ (——) and SP-$Ni_{34}Zr_{66}$ (· · · · ·); X-ray diffraction (Mo-Kα); pair distribution function $g(R)$.

Table 4. MS-$Ni_{34}Zr_{66}$ and SP-$Ni_{34}Zr_{66}$; coordination numbers.

Specimen	Z_{NiZr}	Z_{ZrZr}
MS-$Ni_{34}Zr_{66}$	5.8	10.8
SP-$Ni_{34}Zr_{66}$	6.1	11.2

Table 5. Warren-Cowley short range order parameters.

Radiation used	Specimen	α	α_{max}	α_{rel}
n	MS-$Ni_{31}Zr_{69}$	−0.08	−0.45	0.18
	MA-$Ni_{30}Zr_{70}$	−0.14	−0.43	0.32
n	MS-$Ni_{63.7}Zr_{36.3}$	−0.25	−0.57	0.44
	MA-$Ni_{65}Zr_{35}$	−0.43	−0.54	0.80
X	MS-$Ni_{34}Zr_{66}$	−0.03	−0.52	0.05
	SP-$Ni_{34}Zr_{66}$	−0.04	−0.52	0.07

4.3.2. SP-$Ni_{34}Zr_{66}$

The sputtered specimen yielded the structure factor shown in Fig. 10 and the pair correlation function presented in Figure 11. The latter yields again Ni–Zr- and Zr–Zr-distances at 2.68 Å and 3.23 Å, respectively.

In Fig. 12 we compare the $g(R)$-curves as obtained with MS-$Ni_{34}Zr_{66}$ and SP-$Ni_{34}Zr_{66}$. Apparently the sputtered specimen shows a more pronounced first maximum and also a splitting up in the second maximum. The coordination numbers are listed in Table 4.

In both specimens we observe about 6 Zr-atoms around each Ni-atom and about 11 Zr-atoms around each Zr-atom. The splitting up of the second maximum in $g(R)$ from the sputtered specimen shows that in the higher coordination spheres the sputtered and the melt-spun specimen have different atomic structures. Moreover, the peaks obtained with the sputtered sample are slighly shifted to large distances. This points to a less dense structure of the sputtered sample compared with the melt-spin sample. Concerning mechanical properties we state the MS-specimen to be ductile whereas the SP-specimen is very brittle as observed in sputtered specimens from various alloy systems.

Many melt spun alloys are ductile but become brittle during a relaxation treatment. This effect was explained by a decrease of the free volume during annealing. Furthermore, it was often observed that relaxed specimens show more pronounced maxima in $g(R)$ [10, 11]. Therefore it is suggested that the SP-$Ni_{34}Zr_{66}$ specimen is in an energetically lower state than the MS-$Ni_{34}Zr_{66}$ specimen.

4.4. Comparison of the Warren-Cowley Short Range Order Parameters

For all six specimens the Warren-Cowley short range order parameter α according to (1) was calculated as well as the maximum short range order parameter

$$\alpha_{max} = -\frac{c_A}{c_B} \quad \text{with} \quad c_A < c_B$$

and the relative short range order parameter

$$\alpha_{rel} = \frac{\alpha}{\alpha_{max}}.$$

α is always negative which means compound forming tendency in all the alloys under investigation. This furthermore means that each Zr atom prefers next Ni-neighbours and vice versa. This tendency, however, is pronounced for the different specimens in a very different way. The MA-specimens show a compound forming tendency which is twice as large as in the MS-specimens. The degree of the short range order in the SP- and MS-specimens, on the other hand, is rather equal.

Furthermore we note that Ni-rich amorphous alloys show a stronger compound forming tendency than the Zr-rich alloys when produced with the same method. This agrees with theoretical calculations reported in [12], where by minimizing the free energy, the partial $S_{CC}(Q)$ structure factor was obtained, with the result that the short range order is larger in the Ni-rich alloys.

5. Conclusion

From the pair correlation functions, the atomic distances, and the coordination numbers follows that amorphous Ni–Zr alloys which were produced by sputtering, melt-spinning, and mechanical alloying show nearly the same neighbourhood in the fist coordination sphere. The quantitative consideration, however, which was done using the short range order parameter, shows that there are differences in the compound forming tendency between the alloys produced by the different methods.

Of course we have to consider the fact that the three production methods are very different: With the MA method the amorphous substance is made from two crystalline elemental powders by milling. With the MS method the starting material is a molten alloy. With the SP method the formation is done from the gas phase.

The different methods yield products which differ in different properties:

i) SP-specimens can be more brittle than MS-specimens.
ii) There are differences in magnetizability [13].
iii) There are differences in the transition temperature of superconductivity [2].
iv) There are differences in the crystallization temperature [2].

From the present work follows that the Ni–Zr alloys as produced by three different methods have very similar atomic arrangements in the first coordination sphere, but differ slightly in the second and higher spheres. We mention that in amorphous $Ni_{63.7}Zr_{36.3}$- as well as in amorphous $Ni_{32}Pd_{52}P_{16}$-alloys after annealing the first coordination spheres showed similar atomic arrangement as in the quenched state [10, 11]. Thus, different methods of preparation and also annealing treatment apparently do not influence substantially the nearest atomic arrangement.

Acknowledgements

Thanks are due to the Institute Laue-Langevin, Grenoble, for allocation of beam time.

[1] P. Lamparter, M. Schaal, and S. Steeb, Inst. Phys. Conf. Ser. No. 101, Proc. Conf. Neutron and X-ray Scattering Complementary Techniques, Kent 1989, p. 51.
[2] L. Schultz and E. Hellstern, Mat. Res. Soc. Symp. Proc. **80,** 3 (1987).
[3] L. Koester and W. B. Jelon, Neutron Diffracton Newsletter (1983).
[4] P. Chieux, R. de Kouchkovsky, and B. Boucher, J. Phys. F: Met. Phys. **14,** 2239 (1984).
[5] W. Hume-Rothery and Y. V. Raynor, The Structure of Metals and Alloys, 3rd ed., Inst. Metals, London 1954, p. 87.
[6] T. Fukanaga, N. Hayashi, N. Watanabe, and K. Suzuki, Rapidly Quenched Metals, Vol. 1 (S. Steeb and H. Warlimont, eds.), Elsevier Science Publishers B.V. 1985, p. 475.
[7] S. Lefebvre, A. Quivy, J. Bigot, Y. Calvayrac, and R. Bellissent, J. Phys. F: Met. Phys. **15,** L99 (1985).
[8] J. H. Hubbell, Wm. J. Veigele, E. A. Briggs, R. T. Brown, D. T. Cromer, and R. J. Howerton, J. Phys. Chem. Ref. Data **4,** 2130 (1975).
[9] D. T. Cromer, Acta Cryst. **18,** 17 (1965).
[10] S. Lefebvre, H. M. Harmelin, A. Quiry, J. Bigot, Y. Calvayrac, and R. Bellissent, Z. Phys. Chem. N.F. **157,** 365 (1988).
[11] M. Schaal, P. Lamparter, and S. Steeb, Z. Naturforsch. **43a,** 1055 (1988).
[12] A. Pasturel, Z. Phys. Chem. N.F. **157,** 53 (1988).
[13] A. W. Weeber, H. Bakker, F. R. de Boer, Europhys. Lett. **2**(6), 445 (1986)